Inorganic Chemistry
Cite This: Inorg. Chem. 2018, 57, 5413−5419
Article
pubs.acs.org/IC

Stabilization Mechanism of the Tetragonal Structure in a Hydrothermally Synthesized $BaTiO_3$ Nanocrystal

Kenta Hongo,[*,†,‡,¶,#] Sinji Kurata,[§] Apichai Jomphoak,[∥] Miki Inada,[⊥] Katsuro Hayashi,[§] and Ryo Maezono[▽,#]

[†]Research Center for Advanced Computing Infrastructure and [▽]School of Information Science, JAIST, Asahidai 1-1, Nomi, Ishikawa 923-1292, Japan

[§]Department of Applied Chemistry, Faculty of Engineering, and [⊥]Center of Advanced Instrumental Analysis, Kyushu University, Fukuoka 819-0395, Japan

[∥]National Electronics and Computer Technology Center, 112 Phahon Yothin, Klong Luang, Pathumthani 12120, Thailand

[¶]National Institute for Materials Science, 1-2-1 Sengen, Tsukuba, Ibaraki 305-0047, Japan

[#]Computational Engineering Applications Unit, RIKEN, 2-1 Hirosawa, Wako, Saitama 351-0198, Japan

[‡]PRESTO, Japan Science and Technology Agency (JST), 4-1-8 Honcho, Kawaguchi, Saitama 332-0012, Japan

Supporting Information

ABSTRACT: Higher OH concentration is identified in tetragonal barium titanate ($BaTiO_3$) nanorods synthesized by a hydrothermal method with a 10 vol % ethylene glycol solvent (Inada, M.; et al. *Ceram. Int.* **2015**, *41*, 5581−5587). This is apparently inconsistent with the known fact that higher OH concentration in the conventional hydrothermal synthesis makes pseudocubic $BaTiO_3$ nanocrystals more stable than the tetragonal one. To understand where and how the introduced OH anions are located and behave in the nanocrystals, we applied ab initio analysis to several possible microscopic geometries of OH locations, confirming the relative stability of the tetragonal distortion over the pseudocubic one because of the preference of trans-type configurations of OH anions. We also performed Fourier transform infrared and X-ray diffraction analysis, all being consistent with the microscopic picture established by the ab initio geometrical optimizations.

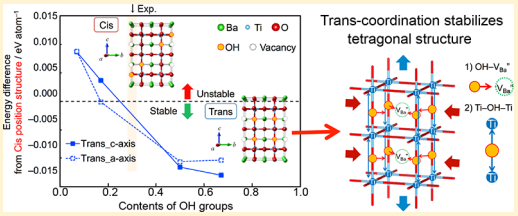

INTRODUCTION

The discovery of a classical ferroelectric barium titanate ($BaTiO_3$) dates back to the 1940s.[1−5] It has a tetragonal structure with a space group symmetry of *P4mm* at room temperature. Much attention has been paid to this material because of a variety of technical applications ranging from condensers to positive temperature coefficient thermistors.[6−9] For example, because of its high dielectric constant, $BaTiO_3$ is used as a dielectric layer of multilayer ceramic capacitors.[8,9]

Hydrothermal synthesis[10] is one of the widely used methods to obtain fine particles of $BaTiO_3$.[11] This method enables us to obtain a highly pure fine powder with small particle size distribution and fairly stoichiometric composition.[12] In the conventional method, however, it is known that it remains difficult to control the crystal orientation (*c* axis in the tetragonal structure) because of the particle size effect[13] and the presence of OH groups in the shell region (surface and outer layer of the crystal),[13,14] yielding pseudocubic nanocrystals[15] rather than tetragonal ones. Extra thermal annealing at around 1300 °C is known to be required to recover the tetragonal structure.[16]

Recently, Inada et al. have reported that a new hydrothermal scheme using 10 vol % ethylene glycol (EG)[11] directly produces tetragonal nanocrystals (c/a = 1.013) without any extra procedures. In the present work, we performed the thermogravimetric analysis applied to the samples and then identified higher OH concentrations inside the 10 vol % EG sample than in the 0 vol % EG one. Doubt immediately arises over our finding because, in the conventional hydrothermal synthesis, the OH inside the $BaTiO_3$ nanocrystals has been widely regarded as having a role in stabilizing the pseudocubic structure.[13] We therefore performed an ab initio lattice relaxation analysis to investigate how the OH substitution stabilizes the tetragonal structure compared with the pseudocubic one.

We have found that the geometrical transition between cis and trans coordination of substituted OH groups depends on their concentrations. The transition modifies Coulombic interactions of the OH substitution with neighboring Ti cations as well as those with Ba vacancies introduced to compensate for charge neutrality. The relaxations due to the above modification can explain the trend of simultaneous contractions along the *a* and *b* axes as well as elongations along the *c* axis when the tetragonal structure is stabilized.

Received: February 10, 2018
Published: April 16, 2018

DOI: 10.1021/acs.inorgchem.8b00381
Inorg. Chem. 2018, 57, 5413−5419

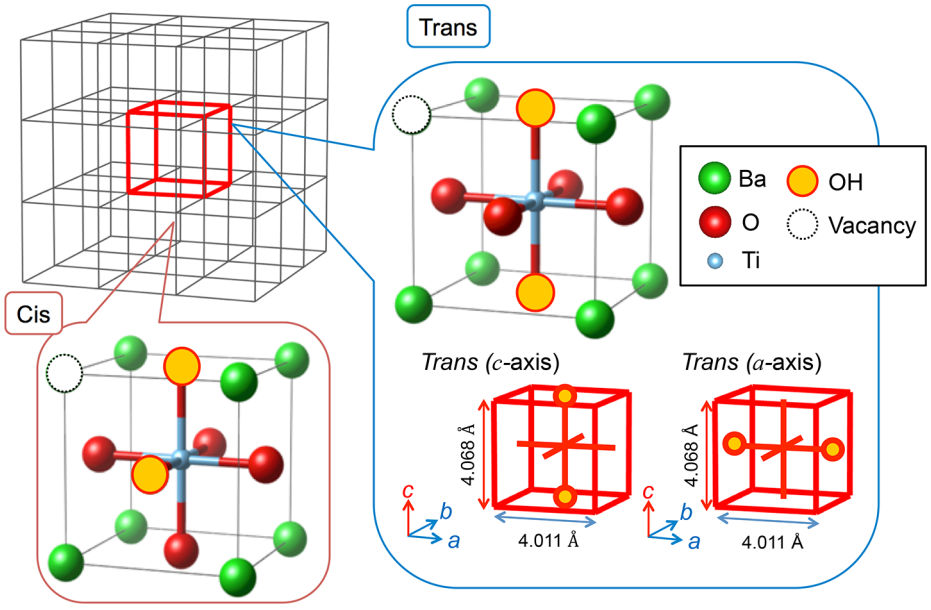

Figure 1. Modeling of 7% OH substitution with cis and trans coordinations by the 3 × 3 × 3 supercell. For the latter, we considered substitutions along the *a* and *c* axes. Lattice constants shown in the figure are fixed at the experimental values obtained by XRD.

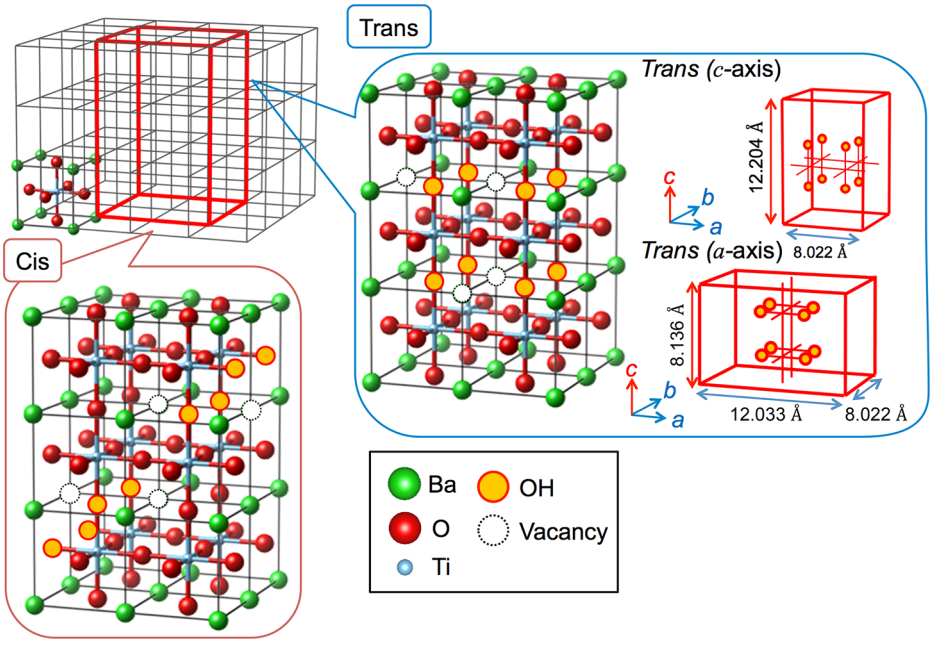

Figure 2. Modeling of 17% OH substitution with cis and trans coordinations by the 4 × 4 × 3 supercell. For the latter, we considered substitutions along the *a* and *c* axes. Lattice constants shown in the figure are fixed at the experimental values obtained by XRD.

EXPERIMENTAL SECTION

Synthesis. $BaTiO_3$ nanocrystals were obtained by hydrothermal synthesis using barium−titanium hydroxide precipitation as a precursor.[11] In the following, we provide minimum descriptions about our synthesis required for understanding further characterizations and theoretical analysis. Detailed information is given in our preceding paper:[11] The concentrations of Ba and Ti in the starting solution were adjusted to 0.3 M (mol L^{-1}) and 0.2 M, respectively. First, 1 M $BaCl_2$ (15 mL) and 2 M $TiCl_4$ (5 mL) solutions were mixed at room temperature, followed by the addition of a 10 M NaOH aqueous solution (10 mL) so as to precipitate barium−titanium hydroxide. In order to obtain 50 mL of the starting slurry, 20 mL of deionized (DI) water or 5 mL (10 vol %) of EG and 15 mL of DI water were added to the mixture. The starting slurry was placed in a 100 mL Teflon-lined stainless steel autoclave and heated in an oven at 200 °C for 24 h, followed by cooling in an ice water. The products were separated, washed by a decantation process repeatedly, and then dried at 60 °C overnight. Hereafter, the samples synthesized by the hydrothermal method with and without EG are denoted as EG-10 and EG-0, respectively. Actually, the nucleation and crystal growth of $BaTiO_3$ occurred via dissolution−reprecipitation. In our previous study,[11] we reported that nucleation was suppressed by the addition of EG. The formation mechanism is also described in the literature.[11]

Characterization. The powder X-ray diffraction (XRD) patterns were collected by an X-ray diffractometer (Bruker AXS) with Cu Kα radiation (40 kV and 40 mA) at room temperature. The lattice parameters were refined by a whole powder pattern decomposition method assuming a *P*4*mm* structural model. The thermal behavior of the products was evaluated by thermogravimetric analysis (TGA). The

DOI: 10.1021/acs.inorgchem.8b00381
Inorg. Chem. 2018, 57, 5413−5419

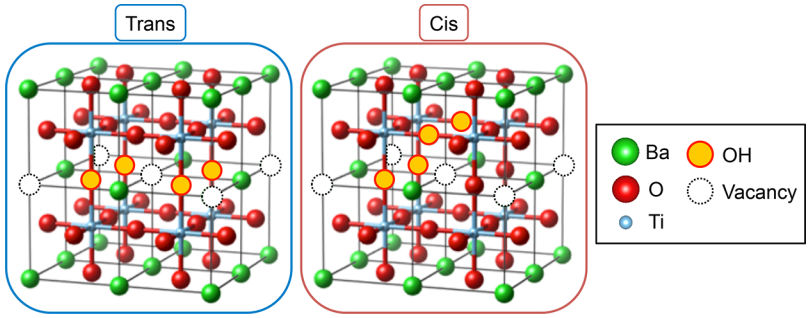

Figure 3. Modeling of 50% OH substitution with cis and trans coordinations by the 2 × 2 × 2 supercell. For the latter, we considered substitutions along the *c* axis.

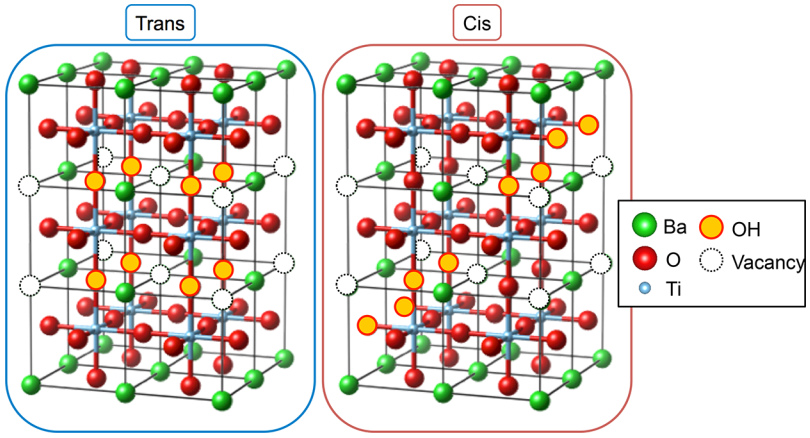

Figure 4. Modeling of 67% OH substitution with cis and trans coordinations by the 2 × 2 × 3 supercell. For the latter, we considered substitutions along the *c* axis.

OH groups were characterized by Fourier transform infrared (FTIR) spectroscopy.

Modeling and Ab Initio Calculations. The present study aims to investigate the stabilization mechanism of the tetragonal structure depending on the OH concentrations. To evaluate the relative stability of $Ba_{1-(1/2)x}TiO_{3-x}(OH)_x$ compounds with different amounts of substitutions *x*, we performed ab initio density functional theory (DFT) simulations with the generalized gradient approximation/Perdew–Burke–Ernzerhof[17] exchange-correlation functional (GGA/PBE), which has been well tested for both the cubic and tetragonal phases of $BaTiO_3$.[18] The amount of OH in synthesized $BaTiO_3$ was estimated from TGA. The experimental results strongly indicated only up to two substitutions, namely, cis and trans coordination, as the possibilities we consider hereafter. The *c*/*a* value, calculated from XRD, of as-synthesized $BaTiO_3$ with EG was bigger than that of pure tetragonal $BaTiO_3$. Also, as-synthesized $BaTiO_3$ included a larger amount of OH than the pure tetragonal structure. These experimental results indicate that the expansion of the *a* axis, which means the incorporation of OH along the *a* axis, is "not in accordance" with the experimental observation that the lattice constants of $Ba_{1-(1/2)x}TiO_{3-x}(OH)_x$ elongate along the *c* axis compared with those of $BaTiO_3$. Thus, we compared only three possibilities of the substitutions, i.e., OH located at the nearest neighbor (cis) or diagonally along the *a* (*c*) axis [*trans-a* (*trans-c*); see Figure 1]. Because of their computability, we considered only four stoichiometric compounds of $Ba_{1-(1/2)x}TiO_{3-x}(OH)_x$ (x = 0.07/0.17/0.50/0.67) within moderately sized simulation cells in which a number of O sites replaced by OH become integers. They were respectively modeled by 3 × 3 × 3, 4 × 4 × 3, 2 × 2 × 2, and 2 × 2 × 3 supercells, i.e., by duplicating the original $BaTiO_3$ unit cell, as shown in Figures 1–4, respectively. To maintain charge neutrality, Ba vacancies have to be introduced (all of the possible patterns of the locations are provided in the Supporting Information). For compensation of the neutrality, the reduction of Ti^{4+} would be another possibility to realize the countercharge for OH substitution. If that were the case, however, the powder color would become blueish, which is not observed in our synthesis. Moreover, in general, Ba vacancies are easily introduced into the $BaTiO_3$ particles when synthesized by a precipitation method because a Ba ion is stable in the alkaline conditions of the reacting solution. These are the reason why we use the models of Ba vacancy and OH substitution. The model structures described above were generated by BIOVIA Materials Studio Visualizer,[19] and then the atomic positions within the simulation cells were further relaxed under the fixed lattice parameters (set as the experimental value).

The geometry optimizations were carried out using the *BFGS* algorithm implemented in CASTEP[20] with thresholds for the energy (1.0×10^{-3} eV cell^{-1}), force (0.05 eV Å^{-1}), stress (0.1 GPa), and displacement (0.002 Å) convergences. Monkhorst–Pack *k*-point meshes of 1 × 1 × 1, 1 × 1 × 1, 2 × 2 × 2, and 2 × 2 × 1 were adopted for the supercells with x = 0.07, 0.17, 0.15, and 0.67, respectively, each of which corresponds to a *k*-point separation of 0.08 Å^{-1}. Ionic cores were described by the on-the-fly ultrasoft pseudopotentials implemented in CASTEP:[20] [He] for O, [Ne] for Ti, and [Kr] $4d^{10}$ for Ba. Kohn–Sham orbitals were expanded in terms of plane waves with E_{cut} = 340 eV, which was determined by the criterion that the total energy converges within 1.0×10^{-4} eV cell^{-1}.

RESULTS AND DISCUSSION

Crystal Structure of the $BaTiO_3$ Nanocrystals and OH in Those Crystals. Figure 5 shows XRD patterns of the with and without ethylene glycol (EG-10 and EG-0) samples. It was confirmed that the samples consist of a major phase of $BaTiO_3$ and a trace impurity of $BaCO_3$, as shown in Figure 5a. The $BaCO_3$ impurity was formed by the reaction between Ba^{2+} and CO_3^{2-} dissolved from the atmosphere. The magnified view of the (200) and (002) reflections shown in Figure 5b reveals that

DOI: 10.1021/acs.inorgchem.8b00381
Inorg. Chem. 2018, 57, 5413–5419

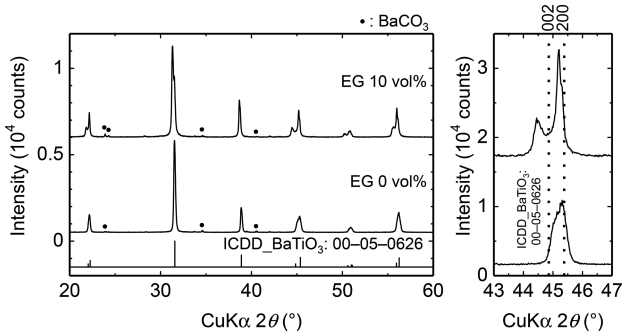

Figure 5. XRD patterns of $BaTiO_3$-synthesized EG-10 and EG-0, respectively. (a) Whole and (b) selected areas that indicate reflections from the (200) planes. The dotted lines show the peak positions of the (200) and (002) directions from ICDD 00-005-0626.

these reflection peaks are clearly separated for the EG-10 sample, while the one broad peak is observed for the EG-0 sample. This means that the EG-10 and EG-0 samples exhibit high and low tetragonality, respectively. It was also found that the diffraction angles of the EG-10 sample are lower than those of the EG-0 sample and bulk $BaTiO_3$ (dotted lines), indicating lattice expansion due to the incorporation of OH groups in the crystals. Figure 6 plots the content of OH groups determined

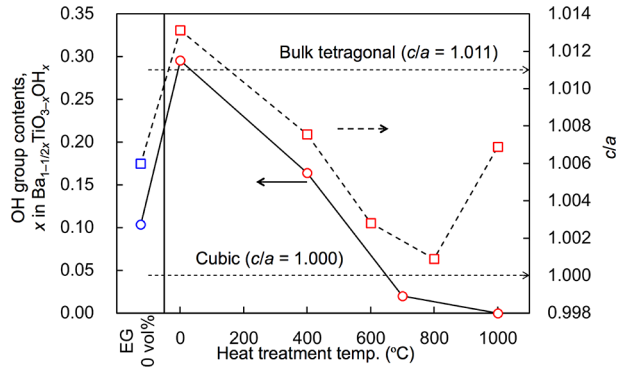

Figure 6. Changes in the OH contents and c/a of $BaTiO_3$ synthesized with 10 vol % EG versus heat-treatment temperature. The blue plots indicate the results without EG.

by TGA along with the c/a ratio as a function of the heat-treatment temperature. The content of OH groups in the EG-10 sample is about 3 times as many as that in the EG-0 sample. The EG-10 sample has a higher c/a ratio than bulk $BaTiO_3$, indicating enhancement of the tetragonality due to the incorporation of OH groups. The OH content and c/a ratio decrease with increasing heat-treatment temperature up to 800 °C, suggesting a significant correlation between the content of OH groups and the c/a ratio of the $BaTiO_3$ crystals.

Characterization of the OH Groups in the Crystals by FTIR and DFT Calculations. FTIR analysis was carried out in order to characterize the OH groups in the crystals. The result is shown in Figure 7. We found a peak at around 3500 cm^{-1}, which can be deconvoluted with a slightly sharp peak at around 3480 cm^{-1} and a broad peak at around 3350 cm^{-1}, indicating that there are two kinds of OH groups in the crystals. The peak area intensity of the EG-10 sample is larger than that of the EG-0 sample; in particular, the area intensity of the peak at around 3480 cm^{-1} is much larger for the EG-10 sample than for the EG-0 sample. As explained later, our DFT gives two different

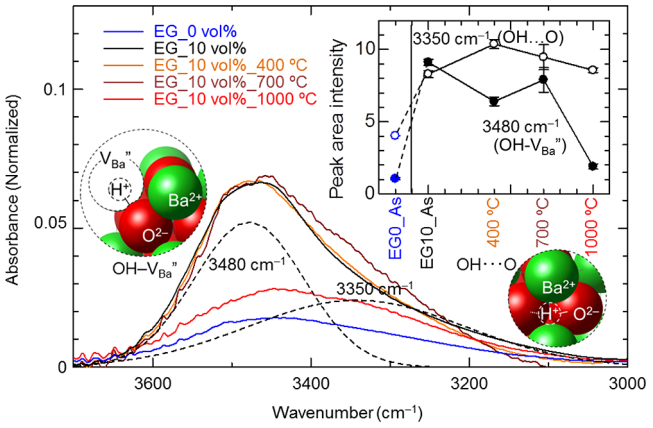

Figure 7. FTIR spectra of the OH groups in the $BaTiO_3$ nanocrystals synthesized with 10 vol % EG before and after heat treatment at 400–1000 °C. For comparison, the result without EG is also shown in the blue line. The peak area intensities versus the heat-treatment temperatures are in the inset.

relaxed positions of substituted OH, which can be identified for each of the peaks, namely, 3480 cm^{-1} being attributed to OH–V_{Ba} defect complexes and 3350 cm^{-1} to OH···O hydrogen bonds. The area intensity of a peak at around 3480 cm^{-1} decreases by heat treatment, as shown in the inset of Figure 7.

Ab Initio Analysis. Ab initio analysis was carried out to gain microscopic insight into how the substituted OH sites play a role in stabilizing the tetragonal crystal structure. As explained in the previous section, we prepared four different supercells to model various substitutions, x. We compared the energies of cis and trans coordinations of OH substituents as a function of x, as shown in Figure 8. We see that the relative stability inverts as the substituent concentration x increases.

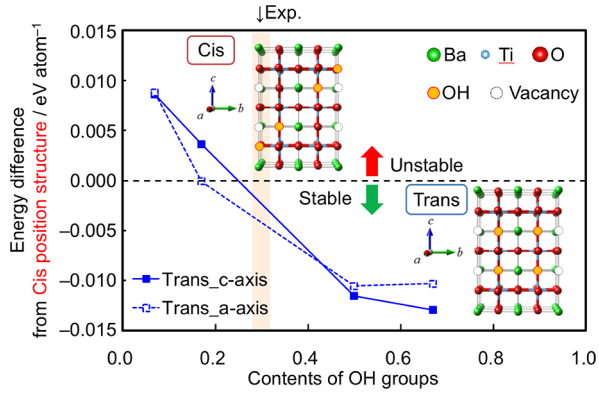

Figure 8. Total energies of the trans coordination along the a and c axes with respect to those of the cis coordination. The region above the broken line indicates that the cis coordination is stable. The region below the broken line indicates that the trans coordination is stable.

The fact that the trans coordination gets more stable for larger x can be roughly connected with the *physical pictures* of the distortion caused by OH substitution. Figures 9 and 10 show how the elongations of the O–Ti–O bond lengths appear around the OH sites with different concentrations, x = 0.07 and 0.5, respectively. While distortion occurs locally around the OH sites for smaller x (Figure 9), it spreads over the whole system uniformly for larger x (Figure 10). The latter has a large enough number of OH sites to get the distortions

DOI: 10.1021/acs.inorgchem.8b00381
Inorg. Chem. 2018, 57, 5413–5419

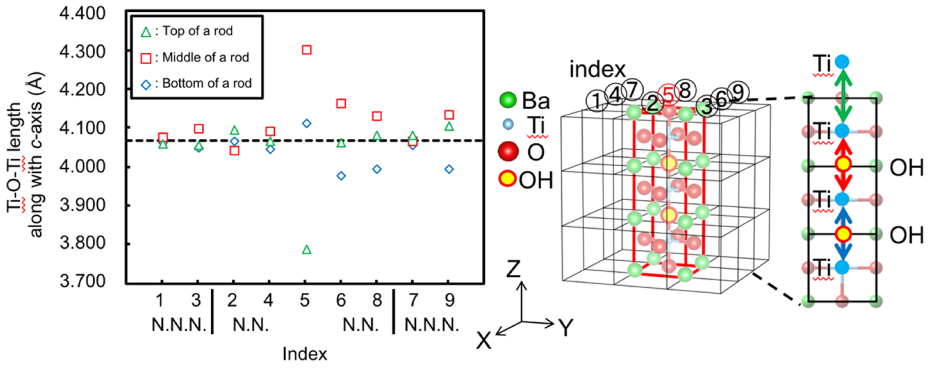

Figure 9. Spatial relaxations of the elongated bond lengths along the *c* axis, evaluated at $x = 0.07$ described by the 3 × 3 × 3 supercell. The right panel gives the convention of indexing for the "rods", $O-Ti^{top}-O-Ti^{center}-O-Ti^{bottom}-O$, along the *c* axis. The upper and lower sides of Ti^{center} at "rod 5" are substituted into OH (trans coordination). The lengths of $O-Ti^{top}-O$, $O-Ti^{center}-O$, and $O-Ti^{bottom}-O$ are plotted in the left panel, showing that the local distortion at the substituted site is relaxed over the nearest neighbors (N.N.) and next-nearest neighbors (N.N.N.).

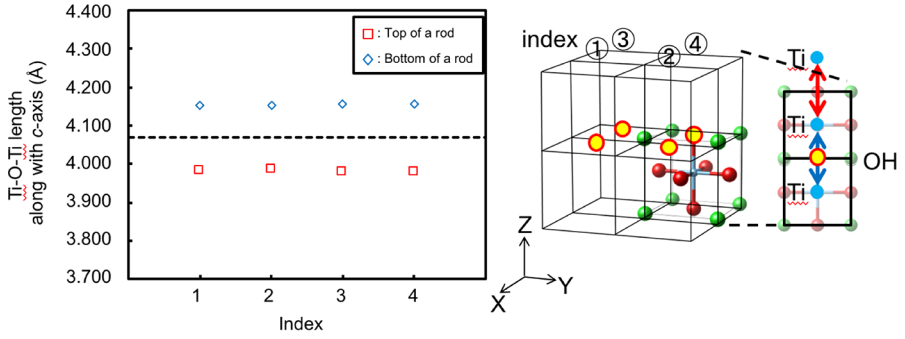

Figure 10. For the larger *x* (OH concentration), distortions due to OH substitutions (changes in the bond lengths along the *c* axis) cooperatively occurring over the crystal. The right panel gives the convention of indexing for the "rods", $O-Ti^{top}-OH-Ti^{bottom}-O$, along the *c* axis. The bond lengths are evaluated at $x = 0.5$ described by the 2 × 2 × 2 supercell, plotted in the left panel over the rods 1–4.

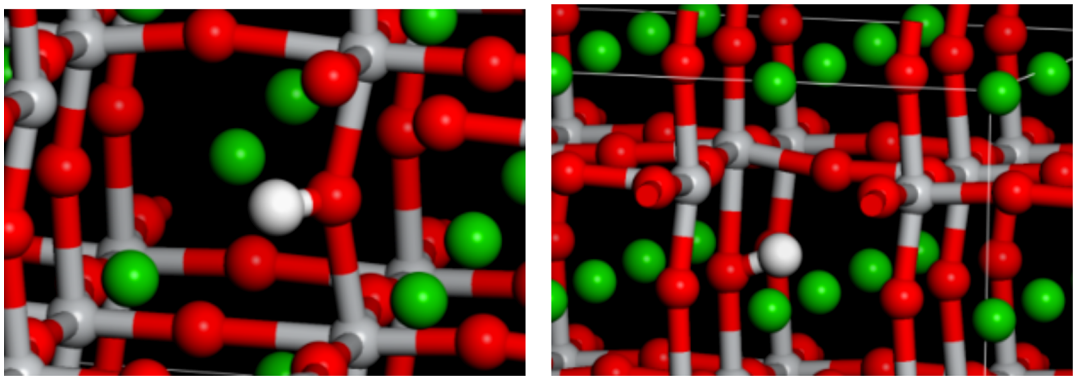

Figure 11. Local relaxations of the atomic positions around the substituted OH, evaluated at $x = 0.07$ described by the 3 × 3 × 3 supercell. White (red) balls represent H (O) atoms. Two cases with and without a Ba vacancy are shown in the left and right panels, respectively. In the former case, the OH site is found to be attracted to the vacancy due to its positively charged background. In the latter case instead, the OH site is attracted to the neighboring O atom to form a hydrogen bond.

cooperatively accommodated within the system, which makes energy loss less than that of the former, where the local distortion causes the energetically unstable state.

Figure 11 shows the lattice relaxation around the substituted OH site, evaluated by the 3 × 3 × 3 supercell with $x = 0.07$. From Figures 9 and 10, we could see two possible effects of distortions caused by the substituents: (a) OH site solely gets attracted by the vacancy V_{Ba}; (b) the trans location of two OH sites along the *c* axis gets the OH–Ti–OH bond elongated along the axis. Effect (a) could be explained by the fact that the vacancy would be charged negatively if the positive Ba^{2+} ion was not there, attracting a proton of a OH ion via electrostatic interactions. Comparing the relaxations of the OH positions with and without V_{Ba} nearby (left and right panels of Figure 11), we can see the formation of the hydrogen bonding between OH and nearest-neighboring O site when without vacancy. This contrast would explain two different absorption peaks in FTIR (Figure 7) at 3480 and 3350 cm^{-1}. The latter peak would be identified as the lattice vibrations with weakened coupling due to the formation of the hydrogen bonding.

Effect (b), elongation of the OH–Ti–OH bond, could be qualitatively understood as a consequence of the weakened

DOI: 10.1021/acs.inorgchem.8b00381
Inorg. Chem. 2018, 57, 5413–5419

electrostatic interaction with Ti caused by replacing O^{2-} with OH^-. The displacement of Ti is, however, found to be small, being around 1.049−1.060 in terms of the ratio of the longer Ti−O bond length to the shorter one (Figure 10). The smaller displacement would be explained as follows: Because the larger displacement of Ti from its original center would yield two larger dipole moments in the opposite direction, the resultant dipole−dipole interactions could give rise to an increase in the system energy. Thus, the possible displacement remains within the smaller amount so as to prevent the system from increasing the energy.

The above effects, (a) attraction of OH by V_{Ba} and (b) elongation of OH−Ti−OH bonds, would explain the trend in the stability of the tetragonal structure relative to the pseudocubic one depending on the OH concentration, x. For the region where cis coordination is stabilized, e.g., $x = 0.07$, the OH sites get attracted to the Ba vacancies individually and uniformly, giving rise to the pseudocubic structure. For the larger x, e.g., $x = 0.25$, where the trans coordination is stabilized instead, effect (a) promotes contraction of the a and b axes (Figure 12), while effect (b) yields elongation along the c axis,

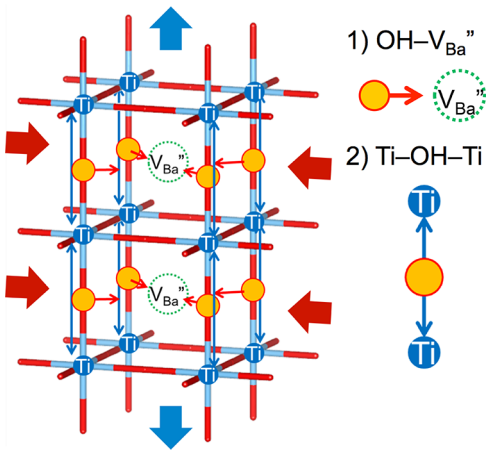

Figure 12. Schematic picture showing how the substituted OH sites stabilize the tetragonal structure with higher concentration. They are attracted to a Ba vacancy, which emerges to realize charge neutrality, yielding contraction of the a and b bond lengths. On top of that, a reduction in the negative stoichiometric charge ($O^{2-} \rightarrow OH^-$) brings about elongation of the bond length along the c axis.

resulting in stabilization of the tetragonal structure. TGA applied to the present EG-synthesized samples estimates $x \sim 0.28$, dropping at the region where the tetragonal structure gets stabilized, consistent with the experimental fact.

The above scenario does not contradict the fact that conventional hydrothermal synthesis gives pseudocubic nanocrystals even with higher x as long as we regard it as the "core−shell" structure,[13] where the doped OH sites are not incorporated into the "core" region but are located only at the "shell" (surface of the core) randomly. The present analysis using supercells corresponds to the assumption that the doped OH sites are located uniformly inside the entire crystal, being the case only for the EG-synthesized sample.

CONCLUSION

We investigated the role of substituted OH in stabilizing the tetragonal anisotropy of the $BaTiO_3$ nanocrystal synthesized by a hydrothermal scheme using EG. TGA was carried out to identify the concentration of OH, revealing that the EG-synthesized sample has around 3 times larger OH concentration compared to the sample systhesized by the conventional hydrothermal scheme. Because in the conventional scheme the introduced OH has been regarded as playing a role in stabilizing the pseudocubic isotropic structure, the present tetragonal anisotropic structure involving the large amount of OH concentration stimulated curiosity.

The apparent contradiction is finally attributed to how the introduced OH groups are distributed throughout a sample. When structural models with uniform OH distributions are employed, our ab initio geometrical relaxation analysis concluded stabilization of the tetragonal anisotropy in the higher OH concentration range where trans coordination of the substitutions was preferred. In the pseudocubic nanocrystals synthesized by the conventional scheme, instead, the introduced OH can be thought of as being distributed only within the "shell" region over the "core" region, not uniformly, and hence the present analysis is beyond the scope of the core−shell interpretation.

The predicted stabilization was explained by several mechanisms such as the cooperative accommodation of the lattice deformations, electrostatic interactions between Ba vacancies and OH, and elongation along trans coordination of the OH sites due to less attraction between the anion site and Ti caused by a reduction in negative charge from O^{2-} to OH^-.

ASSOCIATED CONTENT

Supporting Information

The Supporting Information is available free of charge on the ACS Publications website at DOI: 10.1021/acs.inorgchem.8b00381.

All of the possible patterns of Ba vacancies and OH anions in $Ba_{1-(1/2)x}TiO_{3-x}(OH)_x$ (x = 0.07/0.17/0.50/0.67), as mentioned in Modeling and Ab Initio Calculations (PDF)

AUTHOR INFORMATION

Corresponding Author

*E-mail: kenta_hongo@mac.com.

ORCID

Kenta Hongo: 0000-0002-2580-0907

Katsuro Hayashi: 0000-0002-4413-6511

Notes

The authors declare no competing financial interest.

ACKNOWLEDGMENTS

This work was supported by the Grant-in-Aid for Scientific Research on Innovative Areas "Mixed Anion" project (Grants JP16H06439, JP16H06440, and 17H05478) from MEXT. All of the computations in this work have been performed using the facilities at Research Center for Advanced Computing Infrastructure in JAIST. FTIR analysis was carried out using FTIR620 at the Center of Advanced Instrumental Analysis, Kyushu University. K. Hongo is also grateful for financial support from FLAGSHIP2020 (Projects hp170269 and hp180175 at K-computer), KAKENHI (Grant 17K17762), PRESTO (Grant JPMJPR16NA), and the Materials Research by Information Integration Initiative (MI^2I) project of the Support Program for Starting Up Innovation Hub from JST.

DOI: 10.1021/acs.inorgchem.8b00381
Inorg. Chem. 2018, 57, 5413−5419

R.M. is also grateful for financial support from MEXT-KAKENHI (Grant 16KK0097), FLAGSHIP2020 (Projects hp170269 and hp180175 at K-computer), Toyota Motor Corp., I−O DATA Foundation, and the Air Force Office of Scientific Research (Grant AFOSR-AOARD/FA2386-17-1-4049). K. Hayashi is supported by Elements Strategy Initiative to Form Core Research Center, MEXT, Japan.

REFERENCES

(1) Wainer, E.; Salomon, A. (Titanium Alloy Manufacturing Co.). *Electrical Report 8*; 1942.
(2) Wainer, E.; Salomon, A. (Titanium Alloy Manufacturing Co.). *Electrical Report 9*; 1943.
(3) Ogawa, T. *Busseiron Kenkyu (in Japanese)* **1947**, *6*, 1−27.
(4) Wul, B. Dielectric Constants of Titanates of Metals of the Second Group. *Nature* **1945**, *156*, 480.
(5) Cross, L. E.; Newnham, R. E. *Ceramics and Civilization*; American Chemical Society: Columbus, OH, Vol. *III*, pp 289−305.
(6) Saburi, O. Properties of Semiconductive Barium Titanates. *J. Phys. Soc. Jpn.* **1959**, *14*, 1159−1174.
(7) SABURI, O. Semiconducting Bodies in the Family of Barium Titanates. *J. Am. Ceram. Soc.* **1961**, *44*, 54−63.
(8) Burn, I.; Maher, G. H. High resistivity BaTiO3 ceramics sintered in CO-CO2 atm. *J. Mater. Sci.* **1975**, *10*, 633−640.
(9) Sakabe, Y.; Minai, K.; Wakino, K. High-Dielectric Constant Ceramics for Base Metal Monolithic Capacitors. *Jpn. J. Appl. Phys.* **1981**, *20*, 147.
(10) Pinceloup, P.; Courtois, C.; Leriche, A.; Thierry, B. Hydrothermal Synthesis of Nanometer-Sized Barium Titanate Powders: Control of Barium/Titanium Ratio, Sintering, and Dielectric Properties. *J. Am. Ceram. Soc.* **1999**, *82*, 3049−3056.
(11) Inada, M.; Enomoto, N.; Hayashi, K.; Hojo, J.; Komarneni, S. Facile synthesis of nanorods of tetragonal barium titanate using ethylene glycol. *Ceram. Int.* **2015**, *41*, 5581−5587.
(12) Hayashi, H.; Hakuta, Y. Hydrothermal Synthesis of Metal Oxide Nanoparticles in Supercritical Water. *Materials* **2010**, *3*, 3794−3817.
(13) Hoshina, T.; Wada, S.; Kuroiwa, Y.; Tsurumi, T. Composite structure and size effect of barium titanate nanoparticles. *Appl. Phys. Lett.* **2008**, *93*, 192914.
(14) Petkov, V.; Gateshki, M.; Niederberger, M.; Ren, Y. Atomic-Scale Structure of Nanocrystalline $Ba_xSr_{1-x}TiO_3$ (x = 1, 0.5, 0) by X-ray Diffraction and the Atomic Pair Distribution Function Technique. *Chem. Mater.* **2006**, *18*, 814−821.
(15) Yan, T.; Shen, Z.-G.; Zhang, W.-W.; Chen, J.-F. Size dependence on the ferroelectric transition of nanosized BaTiO3 particles. *Mater. Chem. Phys.* **2006**, *98*, 450−455.
(16) Sasirekha, N.; Rajesh, B. a. Hydrothermal Synthesis of Barium Titanate: Effect of Titania Precursor and Calcination Temperature on Phase Transition. *Ind. Eng. Chem. Res.* **2008**, *47*, 1868−1875.
(17) Perdew, J. P.; Burke, K.; Ernzerhof, M. Generalized Gradient Approximation Made Simple. *Phys. Rev. Lett.* **1996**, *77*, 3865−3868.
(18) Bilc, D. I.; Orlando, R.; Shaltaf, R.; Rignanese, G.-M.; Íñiguez, J.; Ghosez, P. Hybrid exchange-correlation functional for accurate prediction of the electronic and structural properties of ferroelectric oxides. *Phys. Rev. B: Condens. Matter Mater. Phys.* **2008**, *77*, 165107.
(19) *BIOVIA Materials Studio Visualizer*, http://accelrys.com/products/collaborative-science/biovia-materials-studio/, accessed Dec 18, 2017.
(20) Clark, S. J.; Segall, M. D.; Pickard, C. J.; Hasnip, P. J.; Probert, M. I. J.; Refson, K.; Payne, M. C. First principles methods using CASTEP. *Z. Kristallogr. - Cryst. Mater.* **2005**, *220*, 567−570.

DOI: 10.1021/acs.inorgchem.8b00381
Inorg. Chem. 2018, 57, 5413−5419